



# CHORUS

This is the accepted manuscript made available via CHORUS. The article has been published as:

## Negative refraction induced acoustic concentrator and the effects of scattering cancellation, imaging, and mirage

Qi Wei, Ying Cheng, and Xiao-jun Liu

Phys. Rev. B **86**, 024303 — Published 23 July 2012

DOI: [10.1103/PhysRevB.86.024303](https://doi.org/10.1103/PhysRevB.86.024303)

**Negative-refraction induced acoustic concentrator and the effects of scattering  
cancellation, imaging and mirage**

Qi Wei<sup>1</sup>, Ying Cheng<sup>1\*</sup>, and Xiao-jun Liu<sup>1,2†</sup>

<sup>1</sup> Key Laboratory of Modern Acoustics, Nanjing University, Nanjing 210093, China

<sup>2</sup> State Key Laboratory of Acoustics, Institute of Acoustics, Chinese Academy of Sciences,  
Beijing 100190, China

We present a three-dimensional acoustic concentrator capable of significantly enhancing the sound intensity in the compressive region with scattering cancellation, imaging and mirage effects. The concentrator shell is built by isotropic gradient negative-index materials, which together with an exterior host medium slab constructs a pair of complementary medium. The enhancement factor, which can approach infinity by tuning the geometric parameters, is always much higher than that of traditional concentrator made by positive-index materials with the same size. The acoustic scattering theory is applied to derive the pressure field distribution of the concentrator, which is consistent with the numerical full-wave simulations. The inherent acoustic impedance match at the interfaces of the shell as well as the inverse processes of “negative refraction – progressive curvature – negative refraction” for arbitrary sound rays can exactly cancel the scattering of the concentrator. Besides, the concentrator shell can also function as an acoustic spherical magnifying superlens, which produces perfect same-shaped image with bigger geometric and acoustic parameters located at a shifted position. Then some acoustic mirages are observed whereby the waves radiated from (scattered by) an object located in the center region may

seem to be radiated from (scattered by) its image. Based on the mirage effect, we further propose an intriguing acoustic transformer which can transform the sound scattering pattern of one object into another object at will with arbitrary geometric, acoustic and location parameters.

**PACS number(s):** 43.20.+g, 43.35.+d, 42.25.Fx

\* [chengying@nju.edu.cn](mailto:chengying@nju.edu.cn); † [liuxiaojun@nju.edu.cn](mailto:liuxiaojun@nju.edu.cn)

## I. Introduction

In recent years, there has been an increasing attention in the coordinate-transformation method which establishes the correspondence relationship between unprecedented wave manipulations and the required material parameters. Based on the invariance of the wave equation under coordinate transformations, this powerful conceptual design methodology has created a variety of unprecedented effects and functional devices by controlling the propagation paths of classic waves such as matter wave<sup>1</sup>, electromagnetic (EM) wave<sup>2-19</sup> and acoustic wave<sup>20-33</sup> at will. The most intriguing applications enabled by this methodology is cloak, which is capable of reducing the scattering and making an object undetectable.<sup>2-13,20-33</sup> The parameters of the ideal cloak are generally anisotropic, and they can also become isotropic under conformal mapping.<sup>2</sup> With the aid of artificial metamaterials, such cloaks have been experimentally demonstrated at microwave<sup>7</sup> and recently optical frequencies<sup>8,9</sup> in the EM wave field, and at ultrasound<sup>30</sup> and audio frequencies<sup>31</sup> in the acoustic wave field. In subsequent studies, Rahm et al. have further proposed the two-dimensional (2D) cylindrical EM concentrator with positive-index materials, which makes the power flow of incident wave concentrate within the inner compressive region.<sup>13</sup> The proposal is expected to have potential significance in the applications where high intensity field is required.<sup>14-19</sup> Similarly, it is of academic and practical significance to study the analogical concentration of acoustic waves.

In this paper, we propose a three-dimensional (3D) spherical acoustic concentrator, which is constructed by isotropic gradient negative-index materials.<sup>34-37</sup> The key idea in this design is complementary medium which consists of the negative-index shell and a host medium slab

nearby. With the aid of complementary medium, the proposed transformation compresses a bulk of host medium bigger than the concentrator itself into the core region, which finally yields a much higher enhancement factor than that of traditional scheme constructed by positive-index materials. Theoretical analysis based on acoustic scattering theory derivation is performed to demonstrate the concentration and imaging effects of the proposal, which agrees well with the full-wave simulations by finite element method (FEM). The inherent acoustic impedance match at the interfaces cancels the sound scattering of the concentrator. Moreover, the concentrator shell can also perform as an acoustic spherical magnifying superlens<sup>5,35</sup>, in which an object located in the compressive region may produce a perfect same-shaped image with bigger geometric and acoustic parameters positioned at a shifted location. Then the resulting intriguing acoustic mirages<sup>11,38-40</sup> are observed, in which the acoustic waves radiated from (or scattered by) one object may seem to be radiated from (or scattered by) its image. Combining the imaging and the external cloaking<sup>10</sup> effects we further propose an acoustic transformer which can acoustically transform one object into another object at will with arbitrary geometric, acoustic and location parameters.

## II. Modeling

The transformation acoustics yields that, when a space  $x'$  is transformed into another space  $x$ , the bulk modulus tensor  $\kappa(x)$  and the inverse mass density tensor  $\rho^{-1}(x)$  in the new space  $x$  take the form of  $\kappa(x) = \det(A)\kappa'(x')$  and  $\rho^{-1}(x) = A[\rho^{-1}(x')]A^T/\det(A)$ , where  $\kappa'(x')$  and  $\rho^{-1}(x')$  are the modulus tensor and the inverse mass density tensor in the original space  $x'$ , and  $A$  is the Jacobian transformation matrix with components  $A_{ij} = \partial x_i / \partial x'_j$ . For a spherical

coordinate transformation from original space  $x'(r', \theta', \varphi')$  to physical space  $x(r, \theta, \varphi)$ , if the transformation only occurs in  $r$  direction [ $r' = f(r)$ ,  $\theta' = \theta$ ,  $\varphi' = \varphi$ ], the mass density  $\rho$  and bulk modulus  $\kappa$  in the physical space can be obtained as

$$\begin{aligned}\rho[r, \theta, \varphi] &= [\rho_0 f'(r) r^2 / f^2(r), \rho_0 / f'(r), \rho_0 / f'(r)], \\ \kappa[r, \theta, \varphi] &= \kappa_0 r^2 / (f'(r) f^2(r)),\end{aligned}\tag{1}$$

where  $\kappa_0$  and  $\rho_0$  are the bulk modulus and mass density of original homogeneous isotropic space. Note that in the study of acoustic properties of materials, the term “isotropic” means having identical values of elastic modulus and mass density in all directions. It can be noticed in Eq. (1) that the three components of bulk modulus  $\kappa$  are equal, which means the bulk modulus of transformation medium is isotropic. On contrary, the three components of mass density  $\rho$  are unequal, which means the mass density of transformation medium is generally anisotropic. However, if the  $r$ -component of mass density is set to be equal with  $\theta$ -component and  $\varphi$ -component, namely  $\rho_0 f'(r) r^2 / f^2(r) = \rho_0 / f'(r)$ , the mass density of transformation medium becomes isotropic too. By solving this differential equation, the general solution which leads to isotropic transformation medium can be expressed as

$$f(r) = tr^{\pm 1},\tag{2}$$

where  $t$  is unknown coefficient which can be obtained by the requirement of continuous condition of  $f(r)$  at boundary.

Figure 1(a) illustrates the schematic configuration of the proposed 3D acoustic concentrator. Its cross section in  $r$ - $\theta$  plane is shown in Fig. 1(b) due to the spherical symmetry. The whole system consists of the compressive region  $A$ , the concentrator shell  $B$  with inner (outer) radius  $a$  ( $b$ ), and the host medium  $C+D$  outside the concentrator. As is shown in Fig.

1(c), the design begins with a radial mapping in spherical coordinate from virtual space  $x'(r', \theta, \varphi)$  to physical space  $x(r, \theta, \varphi)$ :

$$r' = f(r) = \begin{cases} r, & r > b \\ b^2/r, & a < r < b. \\ rb^2/a^2, & r < a \end{cases} \quad (3)$$

The general host medium ( $r > b$ ) is homogeneous isotropic medium such as water and air, and is characterized by the bulk modulus  $\kappa_0$  and mass density  $\rho_0$ . By inserting the transformation functions described by Eq. (3) into Eq. (1), we obtain the material parameters (bulk modulus  $\kappa$  and mass density  $\rho$ ) of the proposed system as

$$[\kappa, \rho] = \begin{cases} [\kappa_0, \rho_0], & r > b \\ [-\kappa_0(r/b)^6, -\rho_0(r/b)^2], & a < r < b. \\ [\kappa_0(a/b)^6, \rho_0(a/b)^2], & r < a \end{cases} \quad (4)$$

It can be noticed in Eq. (4) that the acoustic parameters of the concentrator shell ( $a < r < b$ ) are radius-dependent and negative. The acoustic impedance matches at the interfaces, resulting in scattering cancellation. At  $r = b$ , the bulk modulus of the shell is  $-\kappa_0$  and the mass density is  $-\rho_0$ , which perfectly matches to host medium; at  $r = a$ , the modulus is  $-\kappa_0(a/b)^6$  and the mass density is  $-\rho_0(a/b)^6$ , which matches to the compressive region. The concentrator shell is isotropic due to the appropriate transformation function  $f(r)=b^2/r$  which satisfies the type described by Eq. (2), and other functions such as the simple linear function  $f(r)=b-(r-b)(b^2/a-b)/(b-a)$  will yield an anisotropic shell. The compressive region is isotropic too since the transformation function  $f(r)=rb^2/a^2$  also satisfies the type of Eq. (2). Besides, the wavelength in the homogeneous compressive region is shorter than that in the host medium because of its smaller bulk modulus and mass density.

The construction of the proposed concentration system can be vividly described as follows.

First, a large sphere of host medium with a radius of  $b^2/a$  in original space [Fig. 2(a)] is compressed into a small sphere with a radius of  $a$  in physical space [Fig. 2(b)], namely the compressive region  $A$ . Such compression leads to higher intensity in compressive region, as discussed in Section III. Then, we fill the empty region  $a < r < b^2/a$  in physical space with double-layered shell constructed by ordinary medium layer  $C$  ( $b < r < b^2/a$ ) and its complementary medium layer  $B$  ( $a < r < b$ ) with gradient negative parameters. We further set the layer  $C$  to be the same as the host medium, and obtain the single-layer concentrator shell with gradient negative isotropic acoustic parameters, as shown in Fig. 2(b). The zero phase delay<sup>12</sup> together with the inherent impedance match under coordinate transformation eventually results in the nearly perfect scattering cancellation effect.

### III. Acoustic concentration with scattering cancellation effect

#### A. Scattering theory derivation

In order to demonstrate the concentration and scattering cancellation effects of the proposed system, we derive the pressure field formulations by using the acoustic scattering theory and spherical wave expansion method. The acoustic pressure  $p_0$  in host medium,  $p_1$  in the shell and  $p_2$  in the compressive region can be expressed in terms of spherical Bessel function  $J_m(kr)$  and Hankel function of the first kind  $H_m^{(1)}(kr)$ :

$$p_l = \sum_{m=0}^{+\infty} [A_{lm} J_m(k_l r) + C_{lm} H_m^{(1)}(k_l r)] P_m(\cos \theta), \quad (5)$$

where  $l=1, 2, 3$ , and  $A_{lm}$ ,  $C_{lm}$  and  $k_l$  are the coefficients of the incident waves, the scattered waves and the wave number in the corresponding regions, respectively.

The pressure field distribution of the system can be easily reconstructed by solving the five

coefficients ( $C_{2m}=0$ ) and substituting them into Eq. (5). The coefficient  $A_{0m}$  is determined by the incident wave. As a concrete example, a plane harmonic pressure wave  $p_{inc} = P_0 e^{i(k_0 r \cos \theta - \omega t)}$  incidents along  $\theta = 0^\circ$  direction with amplitude  $P_0$ . Then the coefficient  $A_{0m}$  takes the form of  $A_{0m} = P_0 (2m+1) i^m$ . Determination of other four unknown coefficients requires the use of continuous scalar acoustic pressure and radial velocity  $v_r = (i / \omega \rho)(\partial p / \partial r)$  at the interfaces of  $r = a$  and  $r = b$ , which finally yields

$$A_{2m} = A_{1m} = A_{0m}, \quad C_{0m} = C_{1m} = 0. \quad (6)$$

We note that  $C_{0m}=0$  in Eq. (6) demonstrates the effect of scattering cancellation in the host medium for arbitrary acoustic incident waves. Substituting the coefficients of Eq. (6) into Eq. (5), we further obtain

$$p_2(r, \theta) = p_1(a^2/r, \theta) = p_0(rb^2/a^2, \theta), \quad 0 < r < a. \quad (7)$$

Equation (7) shows that the pressure at  $(r, \theta)$  in the compressive region is exactly equal to that at  $(a^2/r, \theta)$  in the shell and that at  $(rb^2/a^2, \theta)$  in the host medium, which directly results in the perfect imaging effect of the proposal. The host medium and compressive region are both isotropic and homogeneous, so Eq. (7) also yields the same wavefront shape in the compressive region and host medium. Identical pressure and smaller acoustic impedance produce higher intensity in the compressive region, and the concentration effect is thus induced. Suppose the acoustic intensity in the free space is  $I_0$ , then the intensity in the compressive region can be expressed as  $I_2 = (b/a)^4 I_0$ , namely the intensity enhancement factor of the proposal is

$$\eta = I_2/I_0 = (b/a)^4. \quad (8)$$

It is worthy to point out that, the proposed scheme can achieve much stronger field

intensity with the same radius than the traditional anisotropic positive-index concentrator<sup>13</sup>.

The general constructed transformation function of the latter is  $f_1(r)$ , as shown by red line in

Fig. 1(c):

$$f_1(r) = \begin{cases} r, & r > b \\ \frac{b-c}{b-a}r + \frac{b(c-a)}{b-a}, & a < r < b, \\ rc/a, & r < a \end{cases} \quad (9)$$

After the same calculation process based on scattering theory, the intensity enhancement factor of the traditional concentrator can be obtained as

$$\eta_1 = (c/a)^2. \quad (10)$$

Since  $a < c < b$ , the maximum of  $\eta_1$  is  $(b/a)^2$ , which is obviously smaller than that of the proposed concentrator. The field intensity of the proposal can be further enhanced by increasing the ratio  $b/a$ .

## B. Concentration and scattering cancellation effect

In our following study, we carry out full-wave simulations by the use of FEM to demonstrate the performance of the proposal. In all numerical simulations, the host medium is set as water with  $\kappa_0 = 2.19$  GPa and  $\rho_0 = 998$  kg/m<sup>3</sup>. The acoustic and geometric parameters of the shell are  $\kappa_1 = -\kappa_0(r/b)^6$ ,  $\rho_1 = -\rho_0(r/b)^2$  and  $a = 1.0$  m,  $b = 1.7$  m, respectively. The compressive region has the acoustic parameters of  $\kappa_2 = \kappa_0(a/b)^6$  and  $\rho_2 = \rho_0(a/b)^2$ , which significantly mismatch to that of the host medium. Under these parameters, the analytical intensity enhancement factor  $\eta$  [Eq. (8)] of the proposal is  $(b/a)^4 = 8.3521$ . The spatial frequency of the incident wave is  $k_0 = 2\pi$  and the corresponding wavelength in the host medium is  $\lambda = 1$  m.

We first simulate the case of plane wave incident. A uniform plane harmonic pressure wave

is incident onto the concentrator along  $\theta = 0^\circ$  direction. Figure 3(a) illustrates the acoustic pressure field distribution of the concentrator in  $r$ - $\theta$  plane. As observed, there is no scattering wave outside the concentrator, and the pressure fields outside and inside the shell maintain undisturbed plane wavefronts. The acoustic rays undergo two inverse processes of “negative refraction – progressive curvature – negative refraction”, and finally return to their original directions, as shown by the white curves in Fig. 3(a). For an exterior observer, the acoustic field thus seems to be emitted from the source directly as if there is no concentrator in the host medium. Figure 3(c) illustrates the corresponding acoustic intensity field distribution, in which the white arrows indicate the directions of the power flow. It can be clearly seen that the acoustic waves are concentrated into the compressive region when passing through the shell, and the intensity field in the compressive region is spatially uniform and strongly enhanced. The arrows in Fig. 3(c) show that there are some energy circulating between the shell and the compressive region. Thus the acoustic power flow through the compressive region is higher than that flow through the whole shell, and then the higher intensity enhancement factor is induced.

In order to verify the efficiency of the proposal to different wavefronts, we further investigate its interaction with acoustic spherical waves. Figures 3(b) and 3(d) depict the acoustic pressure field and intensity field distributions in  $r$ - $\theta$  plane for the concentrator under spherical wave irradiation, respectively. Here, a point source is located at (6.0 m,  $180^\circ$ ,  $0^\circ$ ). It is obvious that the spherical wave is undisturbed by the concentrator. The acoustic intensity is strongly enhanced in the compressive region by the concentrator, while keeping the distribution trend unchanged.

In addition, we quantify the concentration performance of the proposal by the acoustic intensity distributions along  $x$  axis, as plotted in Fig. 4. The types of incident wave and the locations of irradiation source in Figs. 4(a) and 4(b) are same with those in Figs. 3(a) and 3(b), respectively. The solid and circle curves stand for the cases of with and without concentrator, respectively. For the case of plane wave incident, the acoustic intensity is spatially invariable and has average value 0.1128 in free space [the circle curve in Fig. 4(a)]. When we put the concentrator in free space, the intensity outside the concentrator is unchanged, while the intensity in the concentrating shell is smoothly enhanced as the radius decreases. The intensity in compressive region is spatially uniform and has average value 0.9426, so the intensity enhancement factor is about 8.3563, which agrees well with the analytical factor. In contrast, for the case of spherical wave incident, the acoustic intensities both in free space and compressive region decrease as the  $x$ -location increases, while the intensity in the concentrating shell is smoothly enhanced too as the radius decreases. However, the intensity in compressive region is still higher than that in the free space. As an example, the intensities at  $(0 \text{ m}, 0^\circ, 0^\circ)$  for free space case and concentrator case in Fig. 4(b) are 0.0369 and 0.3081, yielding a enhancement factor 8.3496. The simulated enhancement factors for both cases are in good agreement with the analytical factor of Eq. (8). The field intensity in the compressive region can be further enhanced by increasing the ratio  $b/a$ , and the enhancement can theoretically diverge to infinity as the radius of the compressive region goes to zero.

#### **IV. Acoustic imaging and mirage effects**

The concentrator can be also regarded as an acoustic spherical magnifying superlens. In

this section, we focus on its imaging effect and the associated mirage effect.

### A. Imaging of point source

Figures 5(a)-5(d) illustrate the transformation function  $r'=f(r)$  given by Eq. (1) and the physical principle of the imaging effect with different source locations. As shown in Fig. 5(a), the transformation maps a point  $(r', \theta', \varphi')$  within the folded space of  $b < r' < b^2/a$  in the virtual space to three points in the physical space. The three points correspond to  $P(r_0, \theta_0, \varphi_0)$  in the compressive region,  $P'(a^2/r_0, \theta_0, \varphi_0)$  inside the shell and  $P'(r_0b^2/a^2, \theta_0, \varphi_0)$  in the host medium. If one point is set as a source then other two points are its real images. According to the reciprocity principle, the positions of source and real images can be exchanged, thus we only discuss the case of source located at  $P$ . Such a perfect acoustic imaging effect is also illustrated by the sound rays in the lower panel of Fig. 5(a). The ray equation in the proposed concentrator shell is

$$\sin(\theta - \alpha) = er/b^2, \quad (11)$$

with  $\alpha$  and  $e$  being two constants determined by the initial conditions. The point source  $P(r_0, \theta_0, \varphi_0)$  radiates sound rays (red curves) and they first go straight in the compressive region. After negative refraction occurs at the inner interface, they travel in plane curves described by Eq. (11) and intersect at  $P'(a^2/r_0, \theta_0, \varphi_0)$  in the shell. Then they undergo the second negative refraction at the outer interface, and go straight in the host medium and intersect at  $P'(r_0b^2/a^2, \theta_0, \varphi_0)$  at last. As a demonstration, Fig. 5(e) shows the pressure field calculated by FEM when a point source  $P$  is located at  $(0.7 \text{ m}, 0^\circ, 0^\circ)$ . The wave can pass through the shell and reach the outside region without changing the wavefront shape. The shell produces the first real image  $P'(1.4298 \text{ m}, 0^\circ, 0^\circ)$  inside the shell and the second real image  $P'(2.0213 \text{ m},$

$0^\circ, 0^\circ$ ) in the host medium, which agrees well with the theoretical prediction. Moreover, the imaging results in an intriguing mirage effect that the acoustic waves in the shell and in the host medium appear to be radiated from the points  $P''$  and  $P'$ , respectively. If we change the position of point source to  $P''$  ( $P'$ ), then the two real images will appear at  $P$  and  $P'$  ( $P$  and  $P''$ ). It is worth pointing out that the precondition of real imaging is  $a^2/b < r_0 < a$ .

In contrast, the transformation only maps a point in the virtual space outside the folded region into one point source  $P(r_0, \theta_0, \varphi_0)$  and a virtual image  $P'(r_0 b^2/a^2, \theta_0, \varphi_0)$  in physical space. For the case of  $a^3/b^2 < r_0 < a^2/b$  the virtual image appears inside the concentrator shell, while for the case of  $r_0 < a^3/b^2$  the virtual image appears in the compressive region, as illustrated in Figs. 5(b) and 5(c), respectively. In the corresponding field distributions shown in Figs. 5(f) and 5(g), a point source  $P$  is located at (0.4 m,  $0^\circ, 0^\circ$ ) and (0.2 m,  $0^\circ, 0^\circ$ ). The exterior observer may find out that the acoustic waves appear to be radiated from the virtual image  $P'(1.1562 \text{ m}, 0^\circ, 0^\circ)$  and  $P'(0.5781 \text{ m}, 0^\circ, 0^\circ)$ , respectively. The virtual images accurately appear at the locations predicted by the theoretical analysis.

## B. Imaging effects of 2D and 3D cases

For convenience to present, we describe an object  $O_j$  by parameters  $[R_j, (r_j, \theta_j, \varphi_j), (\kappa_j, \rho_j)]$ , where  $R_j, (r_j, \theta_j, \varphi_j)$  and  $(\kappa_j, \rho_j)$  show the geometric size parameter, the position parameters and the acoustic parameters (bulk modulus and density), respectively. As discussed above, for an exterior observer a point source  $P(r_0, \theta_0, \varphi_0)$  in the compressive region always produces an image (either a real image or a virtual image) at  $P'(r_0 b^2/a^2, \theta_0, \varphi_0)$ . Based on the same analysis, the imaging effect can be extended to 2D and 3D cases. For an object with parameters  $[R_1, (r_1, \theta_1, \varphi_1), (\kappa_1, \rho_1)]$ , it always has an image with parameters  $[R_1 b^2/a^2, (r_1 b^2/a^2, \theta_1, \varphi_1), (\kappa_1 (b/a)^6,$

$\rho_1(b/a)^2$ ]. Contrasting the parameters of the image with those of the imaged object, it can be found that the image has same shape, bigger geometric size, bigger acoustic parameters and shifted location, which confirms the magnifying imaging effect of the concentrator. Now we first take a plane source (2D case) as an example. For a circular plane source  $A$  with parameters  $[R_1, (r_1, \theta_1, \varphi_1)]$ , it has a real image  $A'$  with parameters  $[R_1b^2/a^2, (r_1b^2/a^2, \theta_1, \varphi_1)]$  when  $a^2/b < r_1 < a$  [as shown in Fig. 5(d)], or a virtual image with parameters  $[R_1b^2/a^2, (r_1b^2/a^2, \theta_1, \varphi_1)]$  when  $r_1 < a^2/b$ . In the corresponding FEM simulation shown in Fig. 5(h), a plane source  $A$  is located at (0.7 m,  $0^\circ$ ,  $0^\circ$ ) with a radius of 0.3 m, and its real image  $A'$  in the host medium appears at (2.0364 m,  $0^\circ$ ,  $0^\circ$ ) with a radius of 0.8549 m, which confirms the magnifying imaging effect of the shell. It is noteworthy that the white flecks in Fig. 5(h) stand for overvalued pressure fields, which are induced by acoustic surface waves propagating along the interface of the left-hand material and right-hand material. The surface waves are excited by acoustic evanescent waves, which carry the subwavelength detail of the object and decay exponentially in any positive-index medium.

We further look into the imaging effect of 3D case. Figures 6(a) and 6(b) show the pressure field distributions in  $r$ - $\theta$  plane for a modified concentrator and a bare object under plane wave incident, respectively. In Fig. 6(a), a cylinder  $O_1$  with a height of 1.3 m, a radius of 0.65 m and acoustic parameters  $(0.0787\kappa_0, 0.3806\rho_0)$  is put in the compressive region at the location of (0.05 m,  $0^\circ$ ,  $0^\circ$ ), while only a bare cylinder  $O_2$  with a height of 3.757 m, a radius of 1.8785 m and acoustic parameters  $(1.9\kappa_0, 1.1\rho_0)$  is located at (0.1445 m,  $0^\circ$ ,  $0^\circ$ ) in the host medium as shown in Fig. 6(b). It can be found that the pressure field distribution outside the dashed circle ( $r = b^2/a$ ) in Fig. 6(a) is same as that in Fig. 6(b). Quantitative analysis is also given in

Fig. 7, which plots the acoustic scattered pressures at the circle of  $r = 5$  m in Figs. 6(a) and 6(b). It is obviously that two curves overlap at most angles, indicating the same scattering pattern of these two cases. In other words, because of the magnifying imaging, an observer outside the circle  $r = b^2/a$  may see a same-shaped object located at a shifted position with bigger geometric and acoustic parameters rather than the actual one embedded in the compressive region.

### C. Acoustic transformer

By combining the external cloaking effect<sup>10</sup> and the imaging effect, we can construct a conceptual device, which may be called acoustic transformer, to acoustically transform one object into another at will. The transformer is implemented by two-step procedure. To completely cancel an object  $O_3$  with parameters  $[R_3, (r_3, \theta_3, \varphi_3), (\kappa_3, \rho_3)]$  in acoustics, we first embed an anti-object  $O_4$  with parameters  $[b^2/R_3, (b^2/r_3, \theta_3, \varphi_3), (-\kappa_3(r/b)^6, -\rho_3(r/b)^2)]$  into the concentrator shell. In this way, the scattering of object  $O_3$  is completely cancelled by the concentrator and its anti-object  $O_4$ . The object  $O_3$ , anti-object  $O_4$  and the concentrator can be also regarded as a complex superlens. Next we embed an arbitrary object  $O_5$  with parameters  $[R_5, (r_5, \theta_5, \varphi_5), (\kappa_5, \rho_5)]$  into the compressive region, then the modified concentrator (concentrator with  $O_3$ ,  $O_4$  and  $O_5$ ) will acoustically look like another object  $O_6$ , which is the perfect magnifying imaging of  $O_5$  with parameters  $[R_5 b^2/a^2, (r_5 b^2/a^2, \theta_5, \varphi_5), (\kappa_5 (b/a)^6, \rho_5 (b/a)^2)]$ . It is worthy to emphasize that the choice of objects  $O_3$  and  $O_5$  is arbitrary, indicating that the transformer can acoustically transform arbitrary object into another object with arbitrary geometric, acoustic and position parameters as long as it is located inside the boundary  $r = b^2/a$ .

We also give FEM simulations to demonstrate how the transformer works. Figure 8 shows the acoustic pressure field distributions while Fig. 9 plots the acoustic scattered pressures at the circle of  $r = 5$  m. In Fig. 8(a), a curved sheet  $O_3$  of a thickness of 0.4 m with acoustic parameters  $(3\kappa_0, 1.5\rho_0)$  to be transformed is positioned between  $2.1 \text{ m} < r < 2.5 \text{ m}$  and  $-20^\circ < \theta < 20^\circ$ . As observed, the plane wave is disturbed by  $O_3$ , which results in backward reflection and shadow. The green square curve in Fig. 9 represents its scattering at  $r = 5$  m. In order to make  $O_3$  acoustically invisible, we modify the concentrator by embedding an anti-object  $O_4$  with acoustic parameters  $[-3\kappa_0(r/b)^6, -1.5\rho_0(r/b)^2]$  between  $1.156 \text{ m} < r < 1.3762 \text{ m}$  and  $-20^\circ < \theta < 20^\circ$  into the shell. In Fig. 8(b) we show the calculated pressure field, and the absence of scattering clearly demonstrates the external cloaking effect, which is also confirmed by the blue triangle curve (nearly zero at all angles) in Fig. 9. Then we put the object  $O_1$  whose parameters are same as those used in Fig. 6(a) in the compressive region, and the simulation result is shown in Fig. 8(c). The pressure field shown in Fig. 8(c) is obviously different with that shown in Fig. 8(a). In contrast, the pressure field outside the dashed circle ( $r = b^2/a$ ) shown in Fig. 8(c) is nearly same as that shown in Fig. 6(b), which indicates that the transformer succeeds in making  $O_3$  acoustically look like  $O_2$ . The overlap of the red circle curve and black solid curve at most angles as shown in Fig. 9 also confirms the successful transforming.

## V. Conclusion

We have presented a 3D acoustic concentrator scheme based on coordinate transformations with gradient negative-refraction material. The key idea in our design is complementary

medium which consists of a host medium slab and the gradient negative-index shell. The consistent analytical derivations and numerical simulations show that the shell can produce much stronger intensity field in the compressive region without scattering and the enhancement factor is obviously bigger than that of traditional concentrator constructed by positive-index materials. Moreover, the negative-index shell can be also regarded as an acoustic superlens, which can produce magnifying image with bigger geometric and acoustic parameters located at a shifted position, resulting in some intriguing acoustic mirages. Based on the imaging effect, we further propose an acoustic transformer which can transform the sound scattering pattern of one object into another. The proposal may have potential applications in acoustics such as harnessing, cloaking, imaging and camouflage.

### **Acknowledgement**

This work was supported by the National Basic Research Program of China under Grant No. 2012CB921504, NSFC (11074124, 11104139 and 10904052), SRFDP 20110091120040, Jiangsu Provincial Natural Science Foundation (BK2011542) and Project Funded by the Priority Academic Program Development of Jiangsu higher education institutions.

## References

- <sup>1</sup> S. Zhang, D. A. Genov, C. Sun, and X. Zhang, *Phys. Rev. Lett.* **100**, 123002 (2008).
- <sup>2</sup> U. Leonhardt, *Science* **312**, 1777 (2006).
- <sup>3</sup> J. B. Pendry, D. Schurig, and D. R. Smith, *Science* **312**, 1780 (2006).
- <sup>4</sup> U. Leonhardt and T. G. Philbin, *Prog. Opt.* **53**, 69 (2009).
- <sup>5</sup> M. Yan, W. Yan, and M. Qiu, *Phys. Rev. B* **78**, 125113 (2008).
- <sup>6</sup> S. A. Cummer, B. I. Popa, D. Schurig, D. R. Smith, and J. B. Pendry, *Phys. Rev. E* **74**, 036621 (2006).
- <sup>7</sup> D. Schurig, J. J. Mock, B. J. Justice, S. A. Cummer, J. B. Pendry, A. F. Starr, and D. R. Smith, *Science* **314**, 977 (2006).
- <sup>8</sup> J. Valentine, J. Li, T. Zentgraf, G. Bartal, and X. Zhang, *Nature Materials* **8**, 568 (2009).
- <sup>9</sup> T. Ergin, N. Stenger, P. Brenner, J. B. Pendry, and M. Wegener, *Science* **328**, 337 (2010).
- <sup>10</sup> Y. Lai, H. Y. Chen, Z. Q. Zhang, and C. T. Chan, *Phys. Rev. Lett.* **102**, 093901 (2009).
- <sup>11</sup> F. Zolla, S. Guenneau, A. Nicolet, and J. B. Pendry, *Opt. Lett.* **32**, 1069 (2007).
- <sup>12</sup> T. Ochiai, U. Leonhardt, and J. C. Nacher, *J. Math. Phys.* **49**, 032903 (2008).
- <sup>13</sup> M. Rahm, D. Schurig, D. A. Roberts, S. A. Cummer, D. R. Smith, and J. B. Pendry, *Photon. Nanostr.* **6**, 87 (2008).
- <sup>14</sup> Y. Luo, H. S. Chen, J. J. Zhang, L. X. Ran, and J. A. Kong, *Phys. Rev. B* **77**, 125127 (2008).
- <sup>15</sup> W. Wang, L. Lin, J. X. Ma, C. T. Wang, J. H. Cui, C. L. Du, and X. G. Luo, *Opt. Express* **16**, 11431 (2008).
- <sup>16</sup> W. X. Jiang, T. J. Cui, Q. Cheng, J. Y. Chin, X. M. Yang, R. P. Liu, and D. R. Smith, *Appl. Phys. Lett.* **92**, 264101 (2008).

- <sup>17</sup> A. D. Yaghjian and S. Maci, *New J. Phys.* **10**, 115022 (2008).
- <sup>18</sup> J. J. Yang, M. Huang, C. F. Yang, Z. Xiao, and J. H. Peng, *Opt. Express* **17**, 19656 (2009).
- <sup>19</sup> K. Zhang, Q. Wu, J. H. Fu, and L. W. Li, *J. Opt. Soc. Am. B* **28**, 1573 (2011).
- <sup>20</sup> G. W. Milton, M. Briane, and J. R. Willis, *New J. Phys.* **8**, 248 (2006).
- <sup>21</sup> S. A. Cummer and D. Schurig, *New J. Phys.* **9**, 45 (2007).
- <sup>22</sup> L. W. Cai and J. Sánchez-Dehesa, *New J. Phys.* **9**, 450 (2007).
- <sup>23</sup> H. Chen and C. T. Chan, *Appl. Phys. Lett.* **91**, 183518 (2007).
- <sup>24</sup> S. A. Cummer, B. I. Popa, D. Schurig, D. R. Smith, J. B. Pendry, M. Rahm, and A. Starr, *Phys. Rev. Lett.* **100**, 024301 (2008).
- <sup>25</sup> A. N. Norris, *Proc. R. Soc. A* **464**, 2411 (2008).
- <sup>26</sup> Y. Cheng, F. Yang, J. Y. Xu and X. J. Liu, *Appl. Phys. Lett.* **92**, 151913 (2008).
- <sup>27</sup> D. Torrent, and J. Sánchez-Dehesa, *New J. Phys.* **10**, 063015 (2008).
- <sup>28</sup> H. Y. Chen, T. Yang, X. D. Luo, and H. R. Ma, *Chin. Phys. Lett.* **25**, 3696 (2008).
- <sup>29</sup> Y. Cheng and X. J. Liu, *Appl. Phys. A* **94**, 25 (2009).
- <sup>30</sup> S. Zhang, C. G. Xia, and N. Fang, *Phys. Rev. Lett.* **106**, 024301 (2011).
- <sup>31</sup> B. I. Popa, L. Zigoneanu, and S. A. Cummer, *Phys. Rev. Lett.* **106**, 253901 (2011).
- <sup>32</sup> A. N. Norris and A. L. Shuvalov, *Wave Motion* **48**, 525 (2011).
- <sup>33</sup> X. F. Zhu, B. Liang, W. W. Kan, X. Y. Zou, and J. C. Cheng, *Phys. Rev. Lett.* **106**, 014301 (2011).
- <sup>34</sup> N. Fang, D. J. Xi, J. Y. Xu, M. Ambati, W. Srituravanich, C. Sun, and X. Zhang, *Nature Mater.* **5**, 452 (2006).
- <sup>35</sup> M. Ambati, N. Fang, C. Sun, and X. Zhang, *Phys. Rev. B* **75**, 195447 (2007).

- <sup>36</sup> Y. Ding, Z. Liu, C. Qiu, and J. Shi, Phys. Rev. Lett. **99**, 093904 (2007).
- <sup>37</sup> S. H. Lee, C. M. Park, Y. M. Seo, Z. G. Wang, and C. K. Kim, Phys. Rev. Lett. **104**, 054301 (2010).
- <sup>38</sup> H. Medwin, *Sounds in the Sea: From Ocean Acoustics to Acoustical Oceanography* (Cambridge University Press, Cambridge, 2005).
- <sup>39</sup> E. Centeno, D. Cassagne, and J.-P. Albert, Phys. Rev. B **73**, 235119 (2006).
- <sup>40</sup> S.-C. S. Lin and T. J. Huang, J. Appl. Phys. **106**, 053529 (2009).

### Figure caption

FIG. 1. (Color online) Acoustic concentrator with gradient negative material: (a) 3D cutaway view; (b) cross section in  $r$ - $\theta$  plane.  $A$ ,  $B$  and  $C+D$  are the compressive region, the concentrator shell, and the host medium, respectively.  $B$  and  $C$  construct complementary medium. (c) The transformation function  $f(r)$  of the proposed concentrator and  $f_1(r)$  of traditional one.

FIG. 2. (Color online) Cross section in  $r$ - $\theta$  plane of spatial coordinate transformation expressed in Eq. (3) for the designed spherical concentrator: (a) original (virtual) space; (b) transformed (physical) space.

FIG. 3. (Color online) Acoustic [(a), (b)] pressure field and [(c), (d)] intensity field distributions in  $r$ - $\theta$  plane of the concentrator under the wave incident from [(a), (c)] plane source and [(b), (d)] point source located at (6.0 m,  $180^\circ$ ,  $0^\circ$ ). The white curves in (a)-(b) are acoustic rays while the white arrows in (c)-(d) indicate the direction of the power flow.

FIG. 4. (Color online) Acoustic intensity distributions along  $x$  axis of free space and concentrator under the wave incident from (a) plane source and (b) point source located at (6.0 m,  $180^\circ$ ,  $0^\circ$ ).

FIG. 5. (Color online) The imaging principle of the concentrator shell: a point source locates inside the region (a)  $a^2/b < r_0 < a$ , (b)  $a^3/b^2 < r_0 < a^2/b$  and (c)  $r_0 < a^3/b^2$ ; and (d) a circular

plane source locates inside the region  $a^2/b < r_0 < a$ . The corresponding demonstration of pressure field distributions in  $r$ - $\theta$  plane: for waves incident from a point source  $P$  located at (e) (0.7 m,  $0^\circ$ ,  $0^\circ$ ), (f) (0.4 m,  $0^\circ$ ,  $0^\circ$ ), (g) (0.2 m,  $0^\circ$ ,  $0^\circ$ ) and (h) a circular plane source  $A$  located at (0.7 m,  $0^\circ$ ,  $0^\circ$ ) with a radius of 0.3 m.

FIG. 6. (Color online) Acoustic pressure field distributions in  $r$ - $\theta$  plane of (a) the concentrator with object  $O_1$ , and (b) the bare object  $O_2$  under plane wave incidence.

FIG. 7. (Color online) Angle-dependence of the scattered pressure for the concentrator with object  $O_1$  and the bare object  $O_2$  under plane wave incidence.

FIG. 8. (Color online) The working principle of the transformer: acoustic pressure field distributions in  $r$ - $\theta$  plane of (a) the bare object  $O_3$ , (b) the concentrator with object  $O_3$  and anti-object  $O_4$ , and (c) the concentrator with object  $O_3$  and anti-object  $O_4$  and object  $O_1$  under plane wave incidence.

FIG. 9. (Color online) Angle-dependence of the scattered pressure for the bare object  $O_3$ , the concentrator with object  $O_3$  and anti-object  $O_4$ , the concentrator with object  $O_3$  and anti-object  $O_4$  and object  $O_1$ , and the bare object  $O_2$  under plane wave incidence.

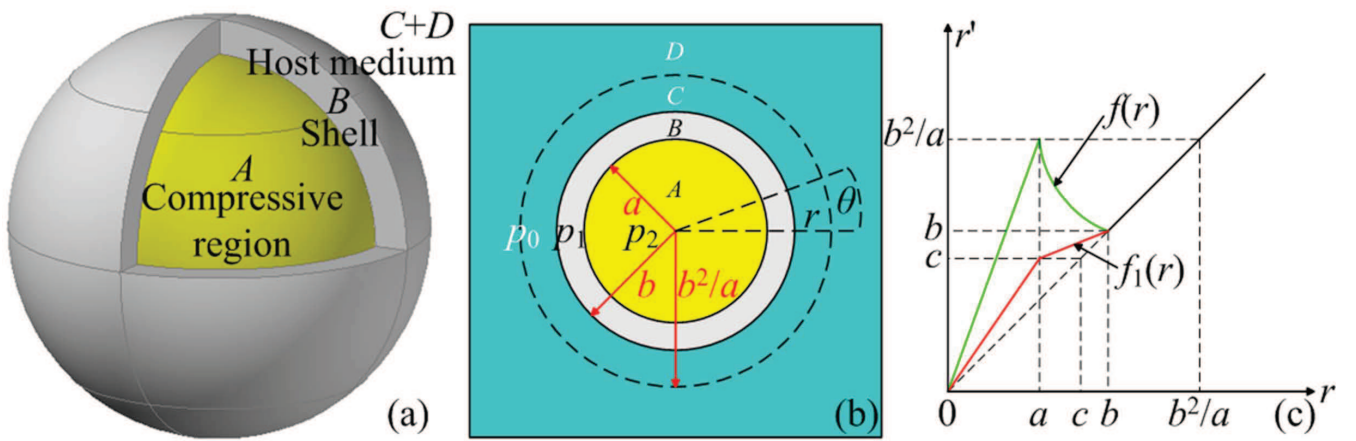


Figure 1

BJ12067

11JUN2012

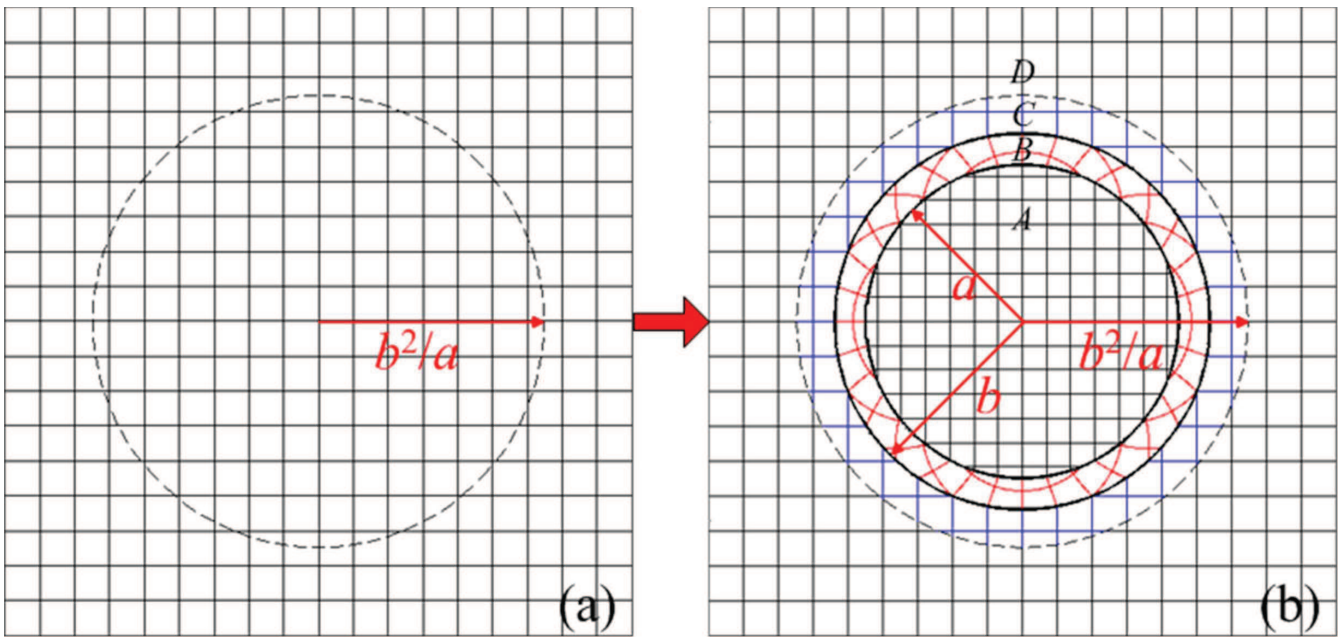


Figure 2 BJ12067 11JUN2012

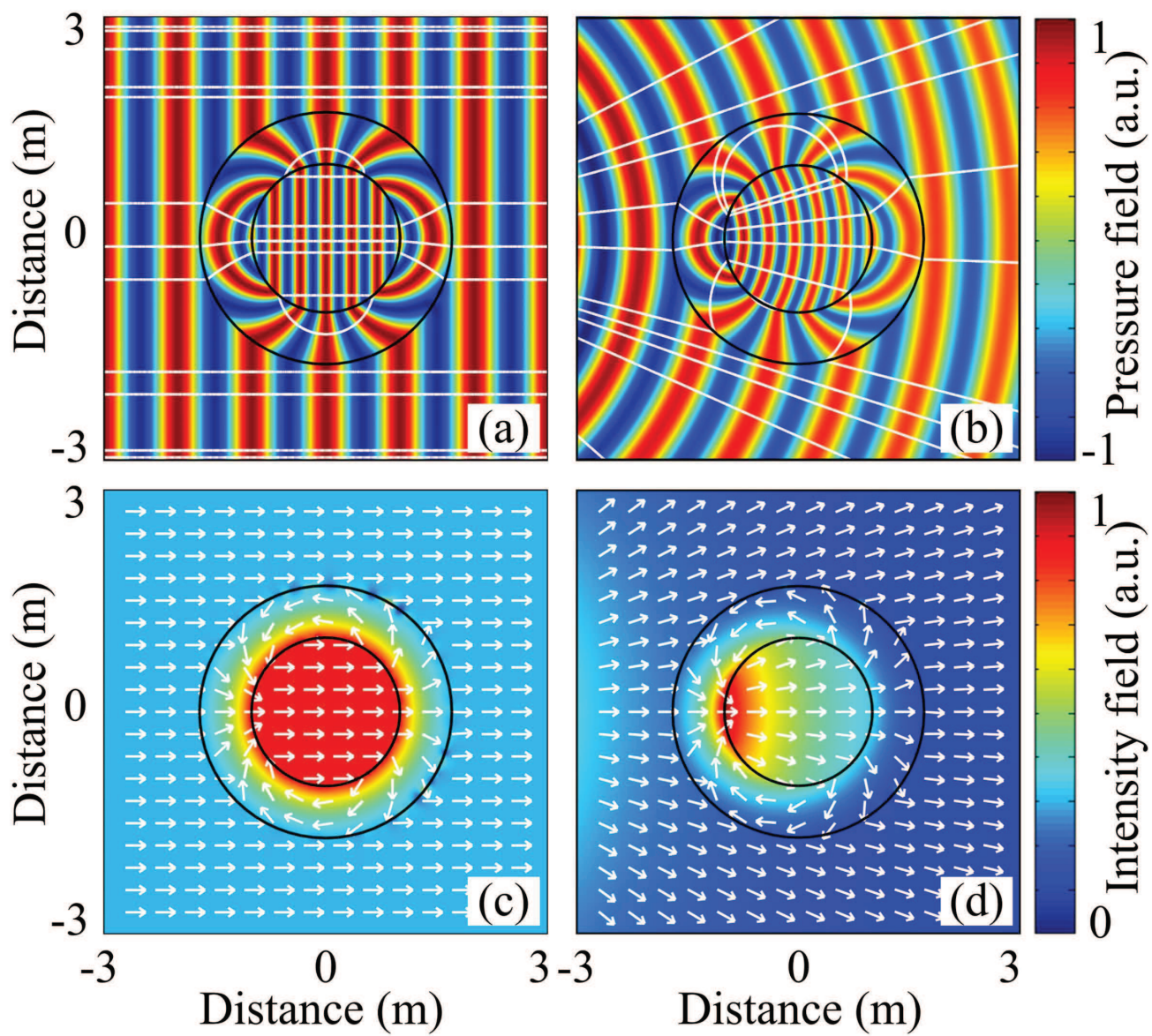


Figure 3

BJ12067

11JUN2012

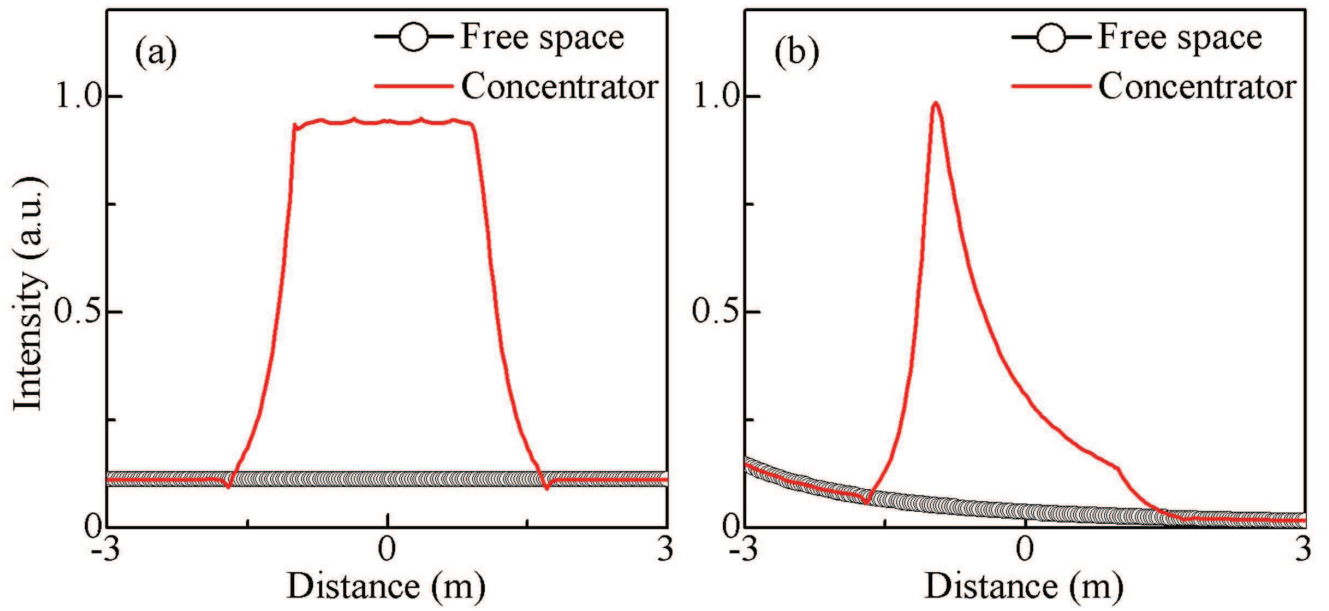


Figure 4 BJ12067 11JUN2012

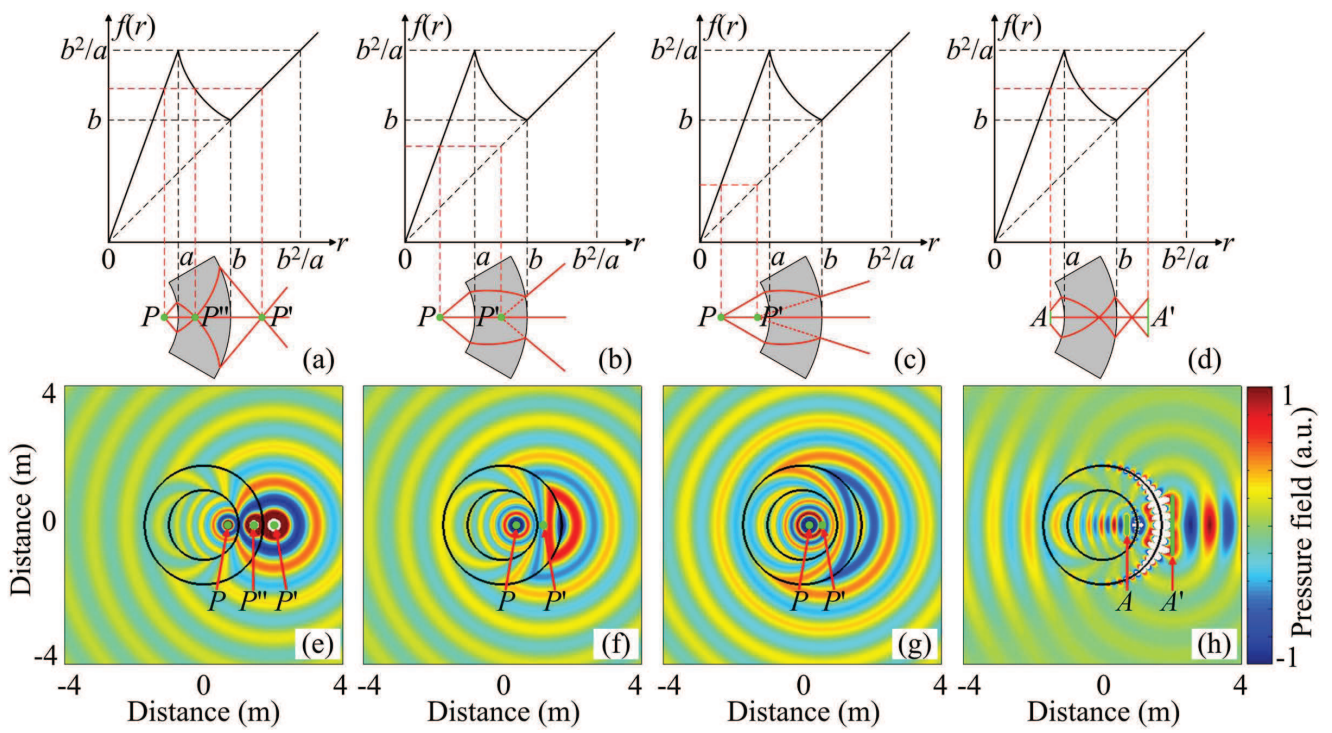


Figure 5 BJ12067 11JUN2012

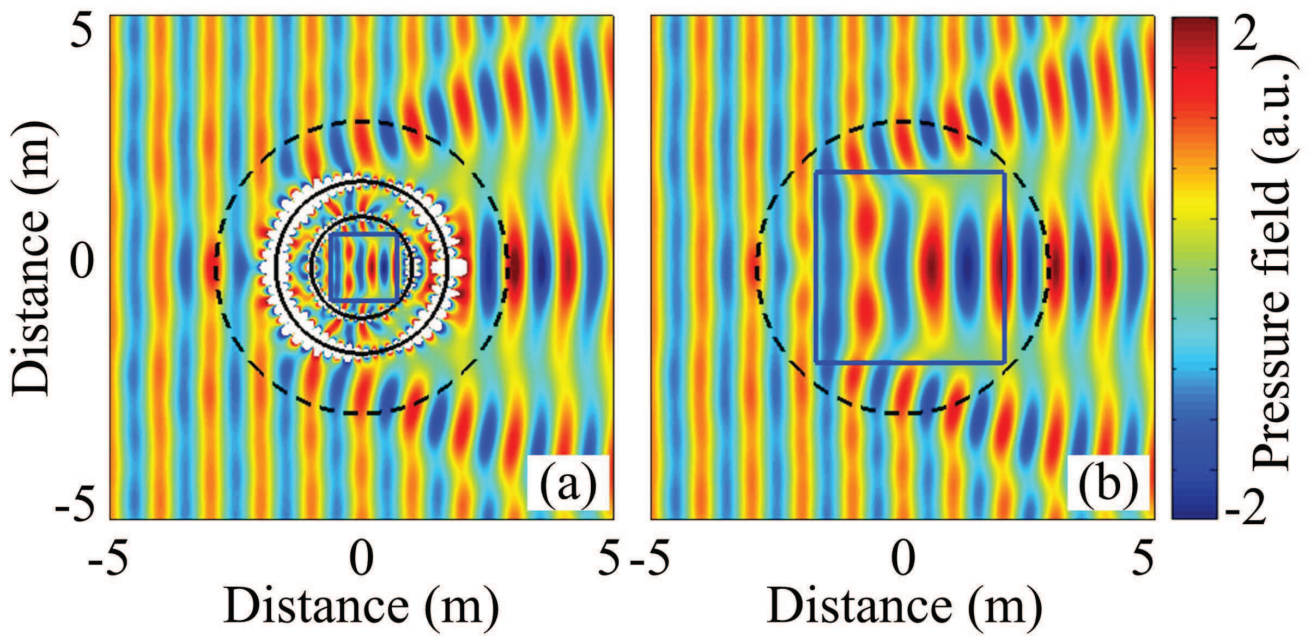


Figure 6

BJ12067

11JUN2012

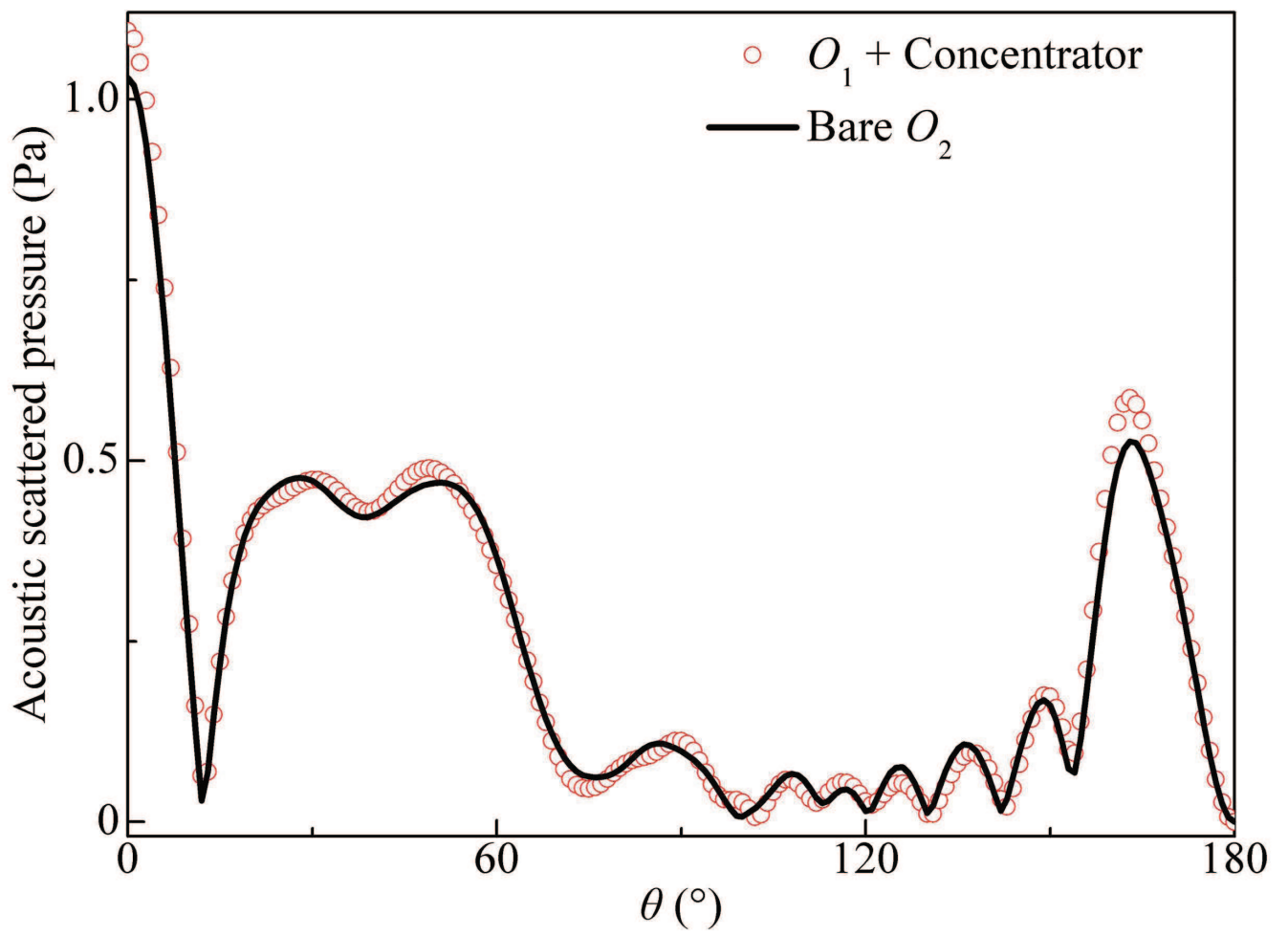


Figure 7

BJ12067

11JUN2012

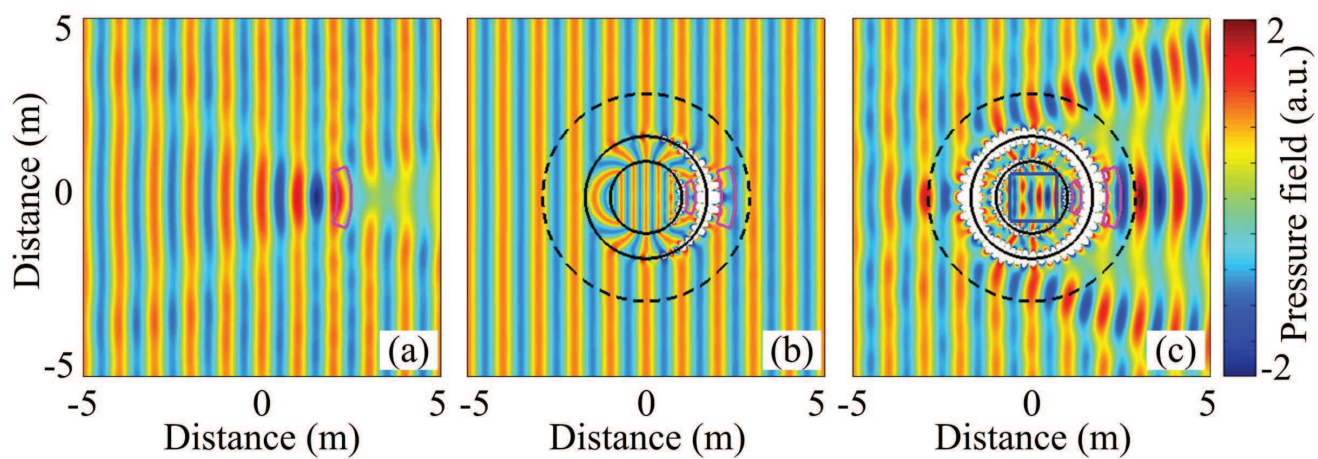


Figure 8

BJ12067

11JUN2012

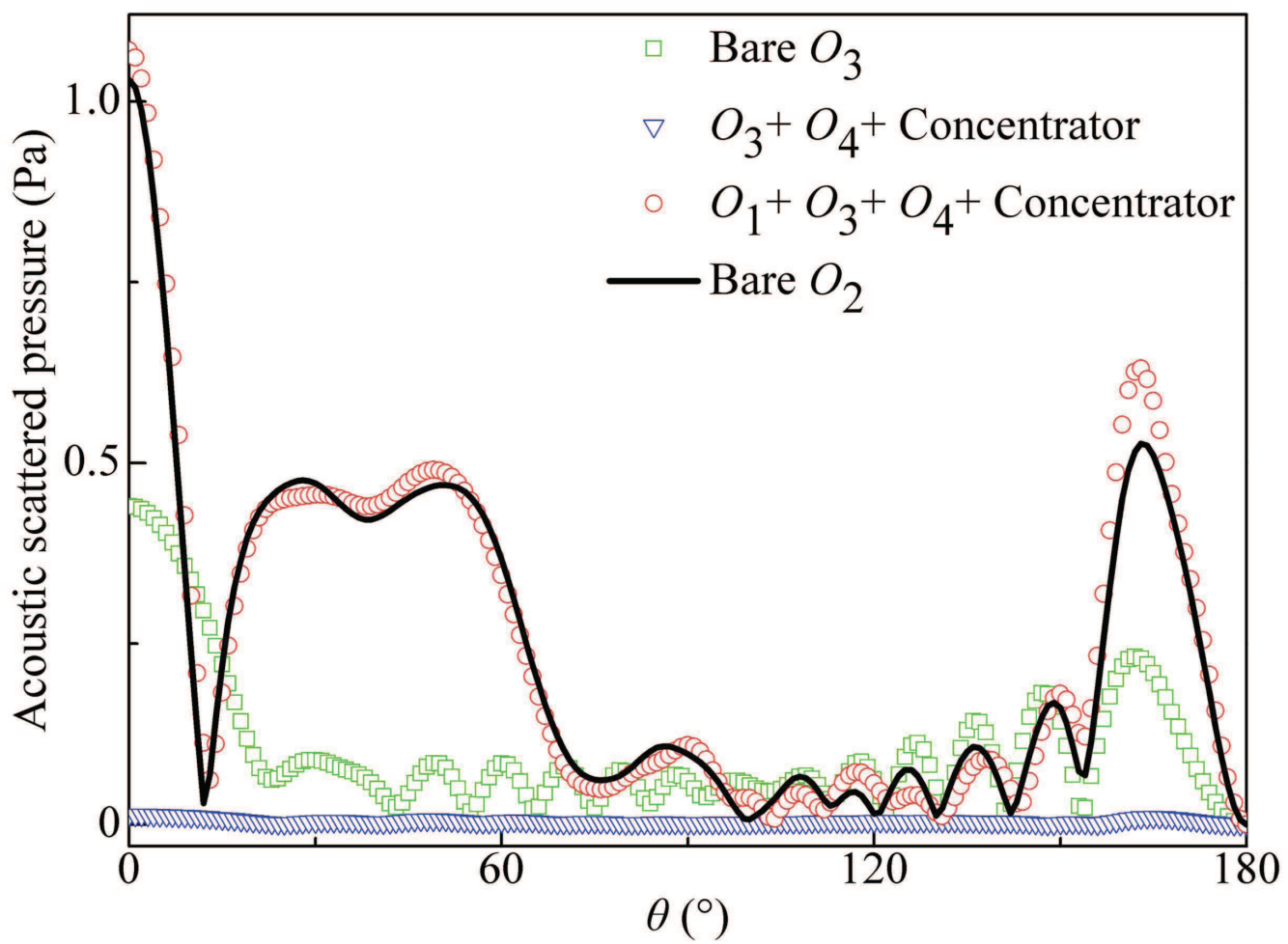


Figure 9

BJ12067

11JUN2012